

Joint Beam Scheduling and Power Allocation for SWIPT in Mixed Near- and Far-Field Channels

Yunpu Zhang, Changsheng You, Weijie Yuan, and Fan Liu

Department of Electronic and Electrical Engineering

Southern University of Science and Technology

Email: zhangyp2022@mail.sustech.edu.cn; {youcs, yuanwj, liuf6}@sustech.edu.cn

Abstract—Extremely large-scale array (XL-array) has emerged as a promising technology to enhance the spectrum efficiency and spatial resolution in future wireless networks, leading to a fundamental paradigm shift from conventional far-field communications towards the new near-field communications. Different from the existing works that mostly considered simultaneous wireless information and power transfer (SWIPT) in the far field, we consider in this paper a new and practical scenario, called *mixed near- and far-field SWIPT*, in which energy harvesting (EH) and information decoding (ID) receivers are located in the near- and far-field regions of the XL-array base station (BS), respectively. Specifically, we formulate an optimization problem to maximize the weighted sum-power harvested at all EH receivers by jointly designing the BS beam scheduling and power allocation, under the constraints on the maximum sum-rate and BS transmit power. To solve this non-convex problem, an efficient algorithm is proposed to obtain a suboptimal solution by leveraging the binary variable elimination and successive convex approximation methods. Numerical results demonstrate that our proposed joint design achieves substantial performance gain over other benchmark schemes without the optimization of beam scheduling and/or power allocation.

Index Terms—Simultaneous wireless information and power transfer (SWIPT), extremely large-scale array (XL-array), mixed near- and far-field channels, beam scheduling, power allocation.

I. INTRODUCTION

Extremely large-scale array/surface (XL-array/surface) has envisioned as a promising technology to achieve super-high spectrum efficiency and spatial resolution for future sixth-generation (6G) wireless networks [1]. With the significant increase of number of antennas, the well-known *Rayleigh distance* will expand to dozens or even hundreds of meters. This thus leads to a fundamental paradigm shift in the electromagnetic (EM) field characteristics, from the conventional far-field communications towards the new *near-field communications* [2], [3].

While most of the existing works have considered either the near- or far-field communications, the *mixed* near- and far-field communications are more likely to appear, in which there exist both near- and far-field users in the network [4]. This means that in a typical communication scenario, the users may be located in the near- or far-field region of the base station (BS), hence leading to more complicated interference issue. Specifically, an interesting observation was unraveled in [4] that due to the energy-spread effect, the near-field user may suffer strong interference from the discrete Fourier transform (DFT)-based far-field beam, when its spatial angle is in the neighborhood of the far-field user angle. On the other hand, such power leakage from the DFT-based far-field beam can also be utilized to efficiently charge the near-field user, leading to the new application of mixed-field simultaneous wireless infor-

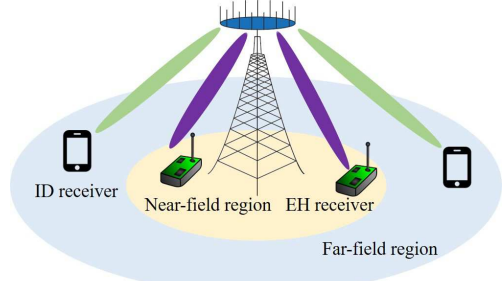


Fig. 1: A mixed near- and far-field SWIPT system.

mation and power transfer (SWIPT) where energy harvesting (EH) and information decoding (ID) receivers are located in the near- and far-field, respectively. However, the design of the mixed-field SWIPT also confronts with new challenges. In particular, thanks to the near-field beam-focusing property [5], the beamforming for the near-field EH receivers should be delicately designed to maximize the EH efficiency, while at the same time, minimizing the interference to the far-field ID receivers. Besides, the beamforming design for the far-field ID receivers should be taken into account the energy-spread effect, which can opportunistically charge the near-field EH receivers when they are located in similar angles. Moreover, the power allocation of the BS should be carefully designed to strike the new *near-and-far* tradeoff in the mixed SWIPT, with the effects of both beam focusing and energy spread taken into account.

To address the above issues, we consider in this paper a new *mixed near- and far-field* SWIPT system as shown in Fig. 1, where the BS equipped with an XL-array simultaneously serves multiple EH and ID receivers, which are located in the near- and far-field regions of the XL-array, respectively. Specifically, our goal is to maximize the weighted sum-power harvested at all EH receivers while ensuring the sum-rate for ID receivers. To this end, we propose a joint BS beam scheduling and power allocation design by utilizing the binary variable elimination and successive convex approximation (SCA) methods. Numerical results demonstrate the effectiveness of the proposed scheme as compared to other benchmark schemes. In particular, we show the necessity of allocating power to the EH receiver in the mixed-field SWIPT, which is in sharp contrast to the conventional far-field SWIPT case, for which all powers should be allocated to ID receivers.

II. SYSTEM MODEL AND PROBLEM FORMULATION

A. System Model

We consider a mixed-field SWIPT system as shown in Fig. 1, where a BS equipped with an N -antenna XL-array simulta-

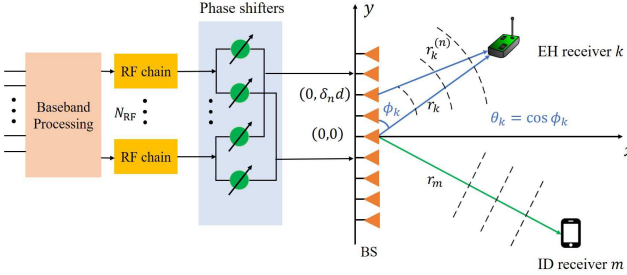


Fig. 2: Illustration of the near and far-field channel models.

neously serves multiple EH and ID receivers. Specifically, K single-antenna EH receivers, denoted by $\mathcal{K} = \{1, 2, \dots, K\}$, are located in the near-field region of the XL-array for enabling high-power energy harvesting, while M single-antenna ID receivers, denoted by $\mathcal{M} = \{1, 2, \dots, M\}$, are assumed to lie in the far-field region of the XL-array with the BS-ID receiver distances larger than the so-called Rayleigh distance, defined as $Z = \frac{2D^2}{\lambda}$ with D and λ denoting the antenna array aperture and carrier wavelength, respectively. For the XL-array BS, it applies the hybrid beamforming architecture to serve $(K + M)$ EH and ID receivers with N_{RF} radio frequency (RF) chains, where $N_{\text{RF}} \geq K + M$.

1) *Near- and Far-Field Channel Models*: In the following, we introduce the channel models for the near-field EH receivers and far-field ID receivers, respectively.

Near-field channel model for EH receivers: For the near-field EH receiver k , its channel from the XL-array BS can be modeled as

$$\mathbf{h}_k^{\text{EH}} = \mathbf{h}_{\text{LoS},k}^{\text{EH}} + \sum_{\ell=1}^{L_k} \mathbf{h}_{\text{NLoS},k,\ell}^{\text{EH}}, \quad k \in \mathcal{K}, \quad (1)$$

where there exist one line-of-sight (LoS) path and L_k non-LoS (NLoS) paths between the BS and EH receiver k . In this paper, we consider SWIPT in high-frequency bands (e.g., mmWave and THz), whose channels are susceptible to blockage. Therefore, we mainly consider the LoS channel component for both EH and ID receivers, while the NLoS components are neglected due to small power [6], [7]. As such, the channel from the BS to EH receiver k can be approximated as $\mathbf{h}_k^{\text{EH}} \approx \mathbf{h}_{\text{LoS},k}^{\text{EH}}$, which is modeled as follows. First, based on the near-field spherical wavefront model in Fig. 2, the distance between the n -th antenna at the BS (i.e., $(0, \delta_n d)$) and EH receiver k is given by

$$r_k^{(n)} = \sqrt{r_k^2 + \delta_n^2 d^2 - 2r_k \theta_k \delta_n d}, \quad (2)$$

where r_k denotes the distance between the BS antenna center and EH receiver k , and $\theta_k = 2d \cos(\phi_k)/\lambda$ denotes the spatial angle at the BS with ϕ_k denoting the physical angle-of-departure (AoD) from the BS center to EH receiver k . Then, by using the second-order Taylor expansion $\sqrt{1+x} \approx 1 + \frac{1}{2}x - \frac{1}{8}x^2$, $r_k^{(n)}$ in (2) can be approximated as $r_k^{(n)} \approx r_k - \delta_n d \theta_k + \frac{\delta_n^2 d^2 (1-\theta_k^2)}{2r_k}$, which is accurate enough when the BS and EH receiver distance r_k is smaller than the Rayleigh distance [6]. As such, the LoS channel between the n -th BS antenna and EH receiver k can be modeled as $[\mathbf{h}_k^{\text{EH}}]_n = h_{k,n}^{\text{EH}} e^{-j2\pi(r_k^{(n)} - r_k)/\lambda}$, where $h_{k,n}^{\text{EH}} = \frac{\lambda}{4\pi r_k^{(n)}}$ is the antenna-wise complex-valued channel gain

of EH receiver k . Moreover, we assume that the EH receivers are located in the radiative Fresnel region for which $r_k > r_{\min} = \max\{\frac{1}{2}\sqrt{\frac{D^3}{\lambda}}, 1.2D\}$ [8]. Under the above assumption, we have $h_{k,1}^{\text{EH}} \approx h_{k,2}^{\text{EH}} \dots \approx h_{k,N}^{\text{EH}} \triangleq h_k^{\text{EH}} = \frac{\lambda}{4\pi r_k}$, where h_k^{EH} is the common complex-valued channel gain for different antennas [5].

Based on the above, the LoS-dominant near-field channel from the BS to EH receiver k can be simply modeled as

$$\mathbf{h}_k^{\text{EH}} \approx \sqrt{N} h_k^{\text{EH}} \mathbf{b}(\theta_k, r_k), \quad k \in \mathcal{K}, \quad (3)$$

where $\mathbf{b}(\theta_k, r_k)$ denotes the (normalized) near-field channel steering vector, which is given by

$$\mathbf{b}(\theta_k, r_k) = \frac{1}{\sqrt{N}} \left[e^{-j2\pi(r_k^{(0)} - r_k)/\lambda}, \dots, e^{-j2\pi(r_k^{(N-1)} - r_k)/\lambda} \right]^T.$$

Far-field channel model for ID receivers: For each ID receiver that is located in the far-field of the BS, say ID receiver m , its channel from the BS can be characterized as below based on the planar wavefront propagation model

$$\mathbf{h}_m^{\text{ID}} = \mathbf{h}_{\text{LoS},m}^{\text{ID}} + \sum_{\ell=1}^{L_m} \mathbf{h}_{\text{NLoS},m,\ell}^{\text{ID}}, \quad m \in \mathcal{M}, \quad (4)$$

where there are one LoS path and L_m NLoS paths between the BS and ID receiver m . By ignoring the negligible NLoS components in high-frequency bands, the BS-ID receiver m channel can be approximated by its LoS component, i.e.,

$$\mathbf{h}_m^{\text{ID}} \approx \sqrt{N} h_m^{\text{ID}} \mathbf{a}(\theta_m), \quad m \in \mathcal{M}, \quad (5)$$

where $h_m^{\text{ID}} = \frac{\lambda}{4\pi r_m}$ represents the complex-valued channel gain of ID receiver m . In addition, $\mathbf{a}(\theta_m)$ denotes the (normalized) far-field channel steering vector, given by

$$\mathbf{a}(\theta_m) \triangleq \frac{1}{\sqrt{N}} \left[1, e^{j\pi\theta_m}, \dots, e^{j\pi(N-1)\theta_m} \right]^T, \quad (6)$$

where θ_m denotes the spatial angle at the BS with ϕ_m denoting the physical AoD from the BS center to ID receiver m .

2) *Signal Model*: Let x_k^{EH} , $k \in \mathcal{K}$ denote the transmitted energy-carrying signal for EH receiver k with power P_k^{EH} and x_m^{ID} , $m \in \mathcal{M}$ the information-bearing signal for ID receivers m with power P_m^{ID} . Then, by applying hybrid beamforming, the transmitted signal vector by the BS is given by $\bar{\mathbf{x}} = \mathbf{F}_A \mathbf{F}_D \mathbf{x}$, where $\mathbf{x} = [x_1^{\text{EH}}, \dots, x_K^{\text{EH}}, x_1^{\text{ID}}, \dots, x_M^{\text{ID}}]^T$, $\bar{\mathbf{x}} = [\bar{x}_1^{\text{EH}}, \dots, \bar{x}_K^{\text{EH}}, \bar{x}_1^{\text{ID}}, \dots, \bar{x}_M^{\text{ID}}]^T$, \mathbf{F}_D represents a $(K+M) \times (K+M)$ digital precoder and \mathbf{F}_A denotes a $N \times (K+M)$ analog precoder. In this paper, to obtain useful insights as well as reduce the hardware cost of the XL-array, we mainly consider the purely analog beamforming design to evaluate the performance gain, for which the digital precoder is set as an identity matrix, i.e., $\mathbf{F}_D = \mathbf{1}_{(K+M), (K+M)}$. To further improve the performance, the weighted minimum mean square error (WMMSE) or zero-forcing (ZF) based digital beamforming can be properly designed given the analog precoder \mathbf{F}_A . The corresponding performance of hybrid beamforming will be evaluated by simulations in Section V.

Let $\mathcal{D} \triangleq \{s_1^{\text{EH}}, \dots, s_K^{\text{EH}}, s_1^{\text{ID}}, \dots, s_M^{\text{ID}}\} \in \mathbb{C}^{K+M}$ denote the beam-scheduling indicator set for the XL-array BS, where s_k^{EH} and s_m^{ID} denote respectively the binary scheduling variable for each EH receiver k and ID receiver m . Specifically, $s_k^{\text{EH}} = 1$ if

$$\text{SINR}_m^{\text{ID}} = \frac{s_m^{\text{ID}} P_m^{\text{ID}} g_m^{\text{ID}} |\mathbf{a}^H(\theta_m) \mathbf{v}_m^{\text{ID}}|^2}{\sum_{k=1}^K s_k^{\text{EH}} P_k^{\text{EH}} g_k^{\text{ID}} |\mathbf{a}^H(\theta_m) \mathbf{v}_k^{\text{EH}}|^2 + \sum_{j=1, j \neq m}^M s_j^{\text{ID}} P_j^{\text{ID}} g_m^{\text{ID}} |\mathbf{a}^H(\theta_m) \mathbf{v}_j^{\text{ID}}|^2 + \sigma_m^2}, \quad (8)$$

EH receiver k is scheduled by the BS and $s_k^{\text{EH}} = 0$ otherwise; while s_m^{ID} is defined in a way similar to s_k^{EH} .

Signal model for far-field ID receivers: Consider the data transmission for a far-field ID receiver m . Its received signal is given by

$$y_m^{\text{ID}} = (\mathbf{h}_m^{\text{ID}})^H \mathbf{v}_m^{\text{ID}} s_m^{\text{ID}} \bar{x}_m^{\text{ID}} + \underbrace{(\mathbf{h}_m^{\text{ID}})^H \sum_{k=1}^K \mathbf{v}_k^{\text{EH}} s_k^{\text{EH}} \bar{x}_k^{\text{EH}}}_{\text{Interference from EH signals}} + \underbrace{(\mathbf{h}_m^{\text{ID}})^H \sum_{j=1, j \neq m}^M \mathbf{v}_j^{\text{ID}} s_j^{\text{ID}} \bar{x}_j^{\text{ID}} + z_m^{\text{ID}}}_{\text{Interference from other ID signals}}, \quad (7)$$

where z_m^{ID} is the received additive white Gaussian noise (AWGN) at ID receiver m with zero mean and power σ_m^2 . As such, the received signal-to-interference-plus-noise ratio (SINR) at ID receiver m is given by (8), as shown at the top of the page, where $g_m^{\text{ID}} = N|h_m^{\text{ID}}|^2$. The corresponding achievable rate in bits per second per Hertz (bps/Hz) is given by $R_m^{\text{ID}} = \log_2(1 + \text{SINR}_m^{\text{ID}})$.

Signal model for near-field EH receivers: For wireless power transfer (WPT), due to the broadcast property of wireless channels, each EH receiver can harvest wireless energy from both the energy and information signals. As a result, by ignoring the negligible noise power at the EH receivers and assuming the linear EH model [9], [10], the harvested power at EH receiver k is given by

$$Q_k = \zeta (s_k^{\text{EH}} |(\mathbf{h}_k^{\text{EH}})^H \mathbf{v}_k^{\text{EH}} \bar{x}_k^{\text{EH}}|^2 + \underbrace{\sum_{i=1, i \neq k}^K s_i^{\text{EH}} |(\mathbf{h}_k^{\text{EH}})^H \mathbf{v}_i^{\text{EH}} \bar{x}_i^{\text{EH}}|^2}_{\text{Harvested power from other EH signals}} + \underbrace{\sum_{m=1}^M s_m^{\text{ID}} |(\mathbf{h}_k^{\text{EH}})^H \mathbf{v}_m^{\text{ID}} \bar{x}_m^{\text{ID}}|^2}_{\text{Harvested power from ID signals}}),$$

where $0 < \zeta \leq 1$ denotes the energy harvesting efficiency.

B. Problem Formulation

In this paper, we assume that the BS has perfect channel state information (CSI) of all EH and ID receivers, i.e., near- and far-field channel steering vectors \mathbf{a} and \mathbf{b} as well as channel gains g_k^{EH} and g_m^{ID} . In practice, this CSI can be efficiently obtained by using existing far-field and near-field channel estimation and beam training methods (see, e.g., [11]–[13]). In addition, for ease of implementation, we assume that if an EH or ID receiver is scheduled, the BS will steer a beam towards it to maximize its received power based on e.g., codebook based beamforming, i.e., $\mathbf{v}_m^{\text{ID}} = \mathbf{a}(\theta_m)$ and $\mathbf{v}_k^{\text{EH}} = \mathbf{b}(\theta_k, r_k)$.

Our objective is to jointly optimize the beam scheduling (i.e., \mathcal{D}) and power allocation (i.e., $\{P_k^{\text{EH}}\}$ and $\{P_m^{\text{ID}}\}$) of the XL-array BS for maximizing the weighted sum-power harvested at all EH receivers, subject to a sum-rate constraint for all ID receivers and a total BS transmit power constraint. Let $\alpha_k \geq 0$ denote a predefined power weight for each EH receiver k , where

a larger value of α_k indicates higher preference for transferring energy to EH receiver k , as compared to other EH receivers. As such, the weighted sum-power transferred to all EH receivers, denoted by Q , can be expressed as

$$Q(\mathcal{D}, \{P_k^{\text{EH}}\}, \{P_m^{\text{ID}}\}) = \sum_{k=1}^K \alpha_k Q_k(\mathcal{D}, \{P_k^{\text{EH}}\}, \{P_m^{\text{ID}}\}).$$

Based on the above, this optimization problem can be formulated as follows

$$\max_{\mathcal{D}, \{P_k^{\text{EH}}\}, \{P_m^{\text{ID}}\}} Q(\mathcal{D}, \{P_k^{\text{EH}}\}, \{P_m^{\text{ID}}\}) \quad (9a)$$

$$\text{s.t.} \quad \sum_{m=1}^M R_m^{\text{ID}}(\mathcal{D}, \{P_k^{\text{EH}}\}, \{P_m^{\text{ID}}\}) \geq R, \quad (9b)$$

$$(\mathbf{P1}) : \quad s_k^{\text{EH}}, s_m^{\text{ID}} \in \{0, 1\}, \quad k \in \mathcal{K}, m \in \mathcal{M}, \quad (9c)$$

$$\sum_{k=1}^K s_k^{\text{EH}} P_k^{\text{EH}} + \sum_{m=1}^M s_m^{\text{ID}} P_m^{\text{ID}} \leq P_0, \quad (9d)$$

$$P_k^{\text{EH}} \geq 0, P_m^{\text{ID}} \geq 0, \quad k \in \mathcal{K}, m \in \mathcal{M}. \quad (9e)$$

Problem (P1) is a mixed-integer optimization problem due to the binary beam-scheduling optimization variables \mathcal{D} in (9c) and the continuous power-allocation variables $\{P_k^{\text{EH}}\}$, $\{P_m^{\text{ID}}\}$ in (9d). Moreover, the beam scheduling and power allocation optimization are strongly coupled in the objective function and the constraints in (9b)–(9d), which renders problem (P1) more difficult to be optimally solved. To tackle these difficulties, we propose an efficient algorithm in this paper to obtain a high-quality solution to problem (P1).

III. PROBLEM REFORMULATION

In this section, we reformulate problem (P1) into a more compact form to facilitate the subsequent algorithm design.

A. Eliminating the Binary Optimization Variables

One of the main challenges in solving problem (P1) arises from the intrinsic coupling between the binary scheduling variables (i.e., s_k^{EH} and s_m^{ID}) and power allocation (i.e., $\{P_k^{\text{EH}}\}$ and $\{P_m^{\text{ID}}\}$), which appear in both the objective function and constraints. To address this issue, we introduce the following variables to eliminate the binary optimization variables

$$\tilde{P}_k^{\text{EH}} = s_k^{\text{EH}} P_k^{\text{EH}}, \quad \tilde{P}_m^{\text{ID}} = s_m^{\text{ID}} P_m^{\text{ID}}. \quad (10)$$

As such, the constraint (9b) can be equivalently transformed into the following form

$$\sum_{m=1}^M R_m^{\text{ID}}(\mathcal{D}, \{P_k^{\text{EH}}\}, \{P_m^{\text{ID}}\}) = \sum_{m=1}^M \tilde{R}_m^{\text{ID}}(\{\tilde{P}_k^{\text{EH}}\}, \{\tilde{P}_m^{\text{ID}}\}), \quad (11)$$

where $\tilde{R}_m^{\text{ID}}(\{\tilde{P}_k^{\text{EH}}\}, \{\tilde{P}_m^{\text{ID}}\})$ is given by (12), as shown at the top of next page. Note that there is a one-to-one correspondence between \tilde{P}_k^{EH} and $\{s_k^{\text{EH}}, P_k^{\text{EH}}\}$. For example, if $\tilde{P}_k^{\text{EH}} > 0$, we have $s_k^{\text{EH}} = 1$ and $P_k^{\text{EH}} = \tilde{P}_k^{\text{EH}}$. Otherwise, if $\tilde{P}_k^{\text{EH}} = 0$, we have $s_k^{\text{EH}} = 0$ and $P_k^{\text{EH}} = 0$. As such, the objective function in (9a) can be expressed in a simpler form, which is given by

$$\tilde{R}_m^{\text{ID}}(\{\tilde{P}_k^{\text{EH}}\}, \{\tilde{P}_m^{\text{ID}}\}) = \log_2 \left(1 + \frac{\tilde{P}_m^{\text{ID}} g_m^{\text{ID}}}{\sum_{k=1}^K \tilde{P}_k^{\text{EH}} g_m^{\text{ID}} |\mathbf{a}^H(\theta_m) \mathbf{b}(\theta_k, r_k)|^2 + \sum_{j=1, j \neq m}^M \tilde{P}_j^{\text{ID}} g_m^{\text{ID}} |\mathbf{a}^H(\theta_m) \mathbf{a}(\theta_j)|^2 + \sigma_m^2} \right). \quad (12)$$

$$\tilde{Q}(\{\tilde{P}_k^{\text{EH}}\}, \{\tilde{P}_m^{\text{ID}}\}) = \sum_{k=1}^K \alpha_k \zeta \left(\tilde{P}_k^{\text{EH}} g_k^{\text{EH}} + \sum_{i=1, i \neq k}^K \tilde{P}_i^{\text{EH}} g_k^{\text{EH}} |\mathbf{b}^H(\theta_k, r_k) \mathbf{b}(\theta_i, r_i)|^2 + \sum_{m=1}^M \tilde{P}_m^{\text{ID}} g_k^{\text{EH}} |\mathbf{b}^H(\theta_k, r_k) \mathbf{a}(\theta_m)|^2 \right). \quad (13)$$

(13), as shown at the top of next page. Similarly, the constraint in (9d) can be rewritten as $\sum_{k=1}^K \tilde{P}_k^{\text{EH}} + \sum_{m=1}^M \tilde{P}_m^{\text{ID}} \leq P_0$.

Based on the above, problem (P1) is equivalently expressed as follows

$$\begin{aligned} & \max_{\{\tilde{P}_k^{\text{EH}}\}, \{\tilde{P}_m^{\text{ID}}\}} \tilde{Q}(\{\tilde{P}_k^{\text{EH}}\}, \{\tilde{P}_m^{\text{ID}}\}) \\ \text{s.t.} \quad & \sum_{m=1}^M \tilde{R}_m^{\text{ID}}(\{\tilde{P}_k^{\text{EH}}\}, \{\tilde{P}_m^{\text{ID}}\}) \geq R, \end{aligned} \quad (14a)$$

$$(\mathbf{P2}) : \quad \sum_{k=1}^K \tilde{P}_k^{\text{EH}} + \sum_{m=1}^M \tilde{P}_m^{\text{ID}} \leq P_0, \quad (14b)$$

$$\tilde{P}_k^{\text{EH}} \geq 0, \tilde{P}_m^{\text{ID}} \geq 0, \quad k \in \mathcal{K}, m \in \mathcal{M}. \quad (14c)$$

B. Correlation Evaluation between EH and ID Receivers

Before solving problem (P2), we first study the correlation between the channels of EH and ID receivers. To this end, we first make a key definition below.

Definition 1. The correlation between any two near-field steering vectors is

$$\eta(\theta_p, \theta_q, r_p, r_q) = |\mathbf{b}^H(\theta_p, r_p) \mathbf{b}(\theta_q, r_q)|. \quad (15)$$

Remark 1. Our prior work [4] studies the correlation between the near- and far-field steering vectors and reveals that the DFT-based far-field beams may cause strong interference to the near-field user even when they locate in different spatial regions. However, when taking a different view from the EH perspective, the power leakage from the DFT-based far-field beams to the near-field user can be used for charging EH devices efficiently. Moreover, it is worth noting that the correlation between near-field steering vectors is a general version of the near-and-far correlation since the far-field channel model is an approximation of the near-field channel model, which is shown below.

Lemma 1. The correlation between any two near-field steering vectors $\eta(\theta_p, \theta_q, r_p, r_q)$ can be approximated as

$$\eta(\theta_p, \theta_q, r_p, r_q) \approx \left| \frac{\hat{C}(\beta_1, \beta_2) + j\hat{S}(\beta_1, \beta_2)}{2\beta_2} \right|, \quad (16)$$

where

$$\beta_1 = \frac{(\theta_q - \theta_p)}{\sqrt{d \left| \frac{1-\theta_p^2}{r_p} - \frac{1-\theta_q^2}{r_q} \right|}}, \quad \beta_2 = \frac{N}{2} \sqrt{d \left| \frac{1-\theta_p^2}{r_p} - \frac{1-\theta_q^2}{r_q} \right|}.$$

Proof: The proof is similar to that in [Lemma 1, [14]] and hence is omitted for brevity. \square

Lemma 1 reveals the correlation of any two near-field steering vectors, which is fundamentally determined by two key parameters β_1 and β_2 . Note that the correlation has a symmetry property, i.e., $\eta(\theta_p, \theta_q, r_p, r_q) = \eta(\theta_q, \theta_p, r_q, r_p)$.

C. Problem Reformulation

Based on Lemma 1, $\tilde{R}(\{\tilde{P}_k^{\text{EH}}\}, \{\tilde{P}_m^{\text{ID}}\})$ in (12) and $\tilde{Q}(\{\tilde{P}_k^{\text{EH}}\}, \{\tilde{P}_m^{\text{ID}}\})$ in (13) can be rewritten as functions of the EH/ID correlation, given by (17) and (18), as shown at the top of next page.

To facilitate the analysis, we first define a correlation matrix as

$$\mathbf{\Lambda} = \begin{bmatrix} \eta_{1,1}^2 & \eta_{1,2}^2 & \cdots & \eta_{1,K+M}^2 \\ \eta_{2,1}^2 & \eta_{2,2}^2 & \cdots & \eta_{2,K+M}^2 \\ \vdots & \ddots & \ddots & \vdots \\ \eta_{K+M,1}^2 & \eta_{K+M,2}^2 & \cdots & \eta_{K+M,K+M}^2 \end{bmatrix}, \quad (19)$$

where $\eta_{p,q}^2$ denotes the correlation between the channel steering vectors of EH/ID receiver p and EH/ID receiver q , which is given by

$$\eta_{p,q}^2 = \begin{cases} |\mathbf{b}^H(\theta_p, r_p) \mathbf{b}(\theta_q, r_q)|^2 & \text{if } 1 \leq p, q \leq K, \\ |\mathbf{b}^H(\theta_p, r_p) \mathbf{a}(\theta_q)|^2 & \text{if } 1 \leq p \leq K, \\ & K+1 \leq q \leq K+M, \\ |\mathbf{a}^H(\theta_p) \mathbf{a}(\theta_q)|^2 & \text{if } K+1 \leq p, q \leq K+M, \\ 1 & \text{if } p = q. \end{cases}$$

Next, to rewrite problem (P2) in a more compact form, we further slightly change the form of the correlation matrix $\mathbf{\Lambda}$ by setting some of the diagonal elements to be zero (i.e., $([\mathbf{\Lambda}]_{(K+1),(K+1)} = 0, \dots, [\mathbf{\Lambda}]_{(K+M),(K+M)} = 0)$), since we do not consider energy harvesting at the ID receivers. As such, the new correlation matrix is given by

$$\bar{\mathbf{\Lambda}} = \begin{bmatrix} 1 & \eta_{1,2}^2 & \cdots & \eta_{1,K+M}^2 \\ \eta_{2,1}^2 & 1 & \cdots & \eta_{2,K+M}^2 \\ \vdots & \ddots & \ddots & \vdots \\ \eta_{K+M,1}^2 & \eta_{K+M,2}^2 & \cdots & 0 \end{bmatrix}. \quad (20)$$

Let $\mathbf{y} = [\tilde{P}_1^{\text{EH}}, \dots, \tilde{P}_k^{\text{EH}}, \dots, \tilde{P}_K^{\text{EH}}, \tilde{P}_1^{\text{ID}}, \dots, \tilde{P}_m^{\text{ID}}, \dots, \tilde{P}_M^{\text{ID}}]^T$ denote the vector including all power allocation optimization variables. Then, problem (P2) can be equivalently recast as follows

$$\begin{aligned} & \max_{\mathbf{y}} \quad (\mathbf{c}^{\text{EH}})^T \bar{\mathbf{\Lambda}} \mathbf{y} \\ \text{s.t.} \quad & \sum_{m=1}^M \log_2 \left(1 + \frac{(\mathbf{c}_m^{\text{ID}})^T \mathbf{y}}{(\mathbf{c}_m^{\text{ID}})^T \bar{\mathbf{\Lambda}} \mathbf{y} + \sigma_m^2} \right) \geq R, \end{aligned} \quad (21a)$$

$$(\mathbf{P3}) : \quad \mathbf{1}_{(K+M) \times 1}^T \mathbf{y} \leq P_0, \quad (21b)$$

$$\mathbf{y} \succeq \mathbf{0}, \quad (21c)$$

where $\mathbf{c}^{\text{EH}} = [g_1^{\text{EH}}, \dots, g_k^{\text{EH}}, \dots, g_K^{\text{EH}}, \mathbf{0}_{1 \times M}]^T$ and $\mathbf{c}_m^{\text{ID}} = [\mathbf{0}_{1 \times K}, \mathbf{0}_{1 \times (m-1)}, g_m^{\text{ID}}, \mathbf{0}_{(m+1) \times M}]^T, \forall m \in \mathcal{M}$.

$$\tilde{R}_m^{\text{ID}}(\{\tilde{P}_k^{\text{EH}}\}, \{\tilde{P}_m^{\text{ID}}\}) = \log_2 \left(1 + \frac{\tilde{P}_m^{\text{ID}} g_m^{\text{ID}}}{\sum_{k=1}^K \tilde{P}_k^{\text{EH}} g_m^{\text{ID}} \eta^2(\theta_m, \theta_k, r_k) + \sum_{j=1, j \neq m}^M \tilde{P}_j^{\text{ID}} g_m^{\text{ID}} \eta^2(\theta_m, \theta_j) + \sigma_m^2} \right), \quad (17)$$

$$\tilde{Q}(\{\tilde{P}_k^{\text{EH}}\}, \{\tilde{P}_m^{\text{ID}}\}) = \sum_{k=1}^K \alpha_k \zeta \left(\tilde{P}_k^{\text{EH}} g_k^{\text{EH}} + \sum_{i=1, i \neq k}^K \tilde{P}_i^{\text{EH}} g_k^{\text{EH}} \eta^2(\theta_k, \theta_i, r_k, r_i) + \sum_{m=1}^M \tilde{P}_m^{\text{ID}} g_k^{\text{EH}} \eta^2(\theta_m, \theta_k, r_k) \right). \quad (18)$$

Compared with problem (P2), problem (P3) renders a more concise form for the joint beam scheduling and power allocation optimization, since the objective function and constraints in (21b) and (21c) are all affine. However, the sum-rate constraint in (21a) is not in a convex form due to the complicated ratio terms as well as the intrinsic coupling between the power allocation. This problem will be solved in the next section.

IV. PROPOSED ALGORITHM FOR SOLVING (P3)

In this section, an efficient algorithm is proposed to obtain a suboptimal solution to problem (P3). Specifically, we first introduce slack variables $\{S_m\}$ and $\{I_m\}$ such that

$$\frac{1}{S_m} = (\mathbf{c}_m^{\text{ID}})^T \mathbf{y}, \quad I_m = (\mathbf{c}_m^{\text{ID}})^T \bar{\Lambda} \mathbf{y} + \sigma_m^2, \quad \forall m \in \mathcal{M}. \quad (22)$$

Then, problem (P3) can be equivalently transformed into the following form

$$\begin{aligned} & \max_{\mathbf{y}, \{S_m\}, \{I_m\}} (\mathbf{c}^{\text{EH}})^T \bar{\Lambda} \mathbf{y} \\ \text{s.t.} \quad & \sum_{m=1}^M \log_2 \left(1 + \frac{1}{S_m I_m} \right) \geq R, \end{aligned} \quad (23a)$$

$$(\mathbf{P4}) : \quad \frac{1}{S_m} \leq (\mathbf{c}_m^{\text{ID}})^T \mathbf{y}, \quad \forall m \in \mathcal{M}, \quad (23b)$$

$$I_m \geq (\mathbf{c}_m^{\text{ID}})^T \bar{\Lambda} \mathbf{y} + \sigma_m^2, \quad \forall m \in \mathcal{M}, \quad (23c)$$

(21b), (21c),

Note that the remaining challenge for solving problem (P4) is the constraint in (23a). To tackle this issue, we first present an useful lemma below.

Lemma 2. Given $x > 0$ and $y > 0$, $f(x, y) = \log_2(1 + \frac{1}{xy})$ is a convex function with respect to x and y .

Proof: The proof is similar to that of [Lemma 1, [15]] and hence is omitted for brevity. \square

Based on Lemma 2, $\log_2(1 + \frac{1}{S_m I_m})$ in (23a) is a joint convex function with respect to S_m and I_m . This thus allows us to apply the SCA method to tackle the constraint (23a) as below.

Lemma 3. By applying the first-order Taylor expansion, $\log_2(1 + \frac{1}{S_m I_m})$ can be lower-bounded as

$$\begin{aligned} \log_2 \left(1 + \frac{1}{S_m I_m} \right) & \geq R_m^{\text{low}} \triangleq \log_2 \left(1 + \frac{1}{\tilde{S}_m \tilde{I}_m} \right) \\ & - \frac{(S_m - \tilde{S}_m)(\log_2 e)}{\tilde{S}_m + \tilde{S}_m^2 \tilde{I}_m} - \frac{(I_m - \tilde{I}_m)(\log_2 e)}{\tilde{I}_m + \tilde{I}_m^2 \tilde{S}_m}, \end{aligned}$$

where $\{\tilde{S}_m, \tilde{I}_m\}$ denote any given feasible points. As such, problem (P4) is approximated as the following problem

$$(\mathbf{P5}) : \quad \max_{\mathbf{y}, \{S_m\}, \{I_m\}} (\mathbf{c}^{\text{EH}})^T \bar{\Lambda} \mathbf{y}$$

$$\text{s.t.} \quad \sum_{m=1}^M R_m^{\text{low}} \geq R, \quad (24a)$$

(21b), (21c), (23b), (23c).

Problem (P5) now is a convex optimization problem, which thus can be efficiently solved via standard solvers such as CVX. Note that the solution obtained from problem (P5) requires an iterative process until the fractional increase of the objective function is below a threshold $\xi > 0$, based on which the optimal beam scheduling and power allocation can be easily recovered.

Remark 2 (Convergence and complexity analysis). First, consider the convergence of the proposed SCA-based algorithm. As problem (P5) is solved optimally in each iteration, the objective value of problem (P5) is non-decreasing. Moreover, since the system sum-power is upper-bounded by a finite value, the proposed algorithm is guaranteed to converge. Next, the overall complexity of the proposed SCA-based algorithm is determined by the number of iterations, denoted by I_{iter} , and the number of the optimization variables (i.e., $K + M$). For each iteration, the computational complexity for solving problem (P5) by the interior-point method can be characterized as $\mathcal{O}((K + M)^{3.5})$. As a result, the total computational complexity of the proposed SCA-based algorithm is $\mathcal{O}(I_{\text{iter}}(K + M)^{3.5})$.

V. NUMERICAL RESULTS

In this section, we present numerical results to demonstrate the effectiveness of the proposed scheme. The considered system model is illustrated in Fig. 3(a), where one BS with $N = 256$ antennas serves three EH receivers and two ID receivers. Specifically, under the polar coordinate, the EH receivers are located at $(0, 0.015Z)$, $(0.1, 0.02Z)$ and $(-0.05, 0.03Z)$, while the two ID receivers are located at $(0, 1.05Z)$ and $(0.05, 1.2Z)$. Unless specified otherwise, we set $P_0 = 30$ dBm, $f = 30$ GHz, $K = 3$, $M = 2$, $\beta = (\lambda/4\pi)^2 = -62$ dB, $\sigma_m^2 = -80$ dBm, $\zeta = 50\%$, $Z = \frac{2D^2}{\lambda} = 327.68$ m, $\xi = 0.001$, $L_k = L_m = 2, \forall k, m$ and $\alpha_k = 1, \forall k \in \mathcal{K}$.

Moreover, for performance comparison, we consider the following four benchmark schemes: 1) *Exhaustive-search scheme*: This scheme enumerates all possible beam scheduling combinations with optimized power allocation, and then selects the best one that achieves the maximum harvested sum-power; 2) *Greedy scheduling + optimized power allocation (GS+OPA) scheme*, for which the EH receiver with the highest EH priority and the ID receiver with the best channel condition are scheduled with optimized power allocation; 3) *Optimal scheduling + equal power allocation (OS+EPA) scheme*, which adopts the optimal beam scheduling and allocates equal power allocation for all selected receivers; 4) *All scheduling + equal power allocation*

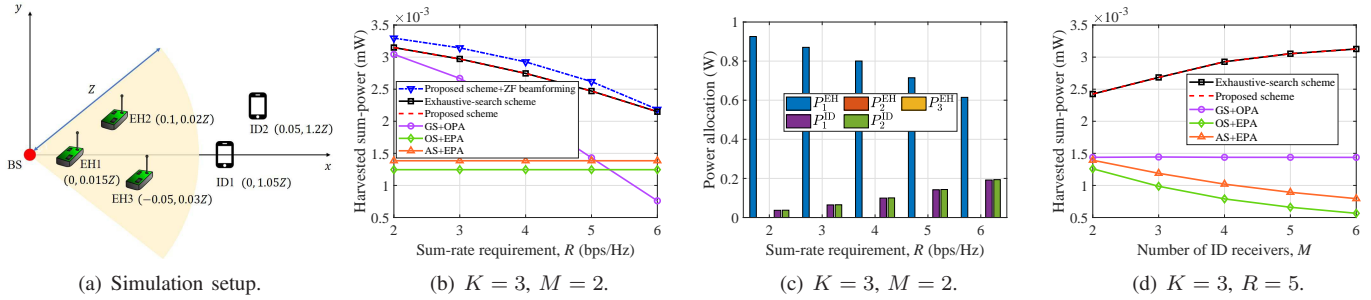


Fig. 3: Simulation setup and harvested sum-power versus system parameters.

(AS+EPA) scheme, for which all EH and ID receivers are scheduled with equal power allocation.

A. Effect of Sum-Rate Requirement

In Fig. 3(b), we compare the harvested sum-powers by different schemes versus the sum-rate requirement, R . First, it is observed that the proposed scheme suffers a small performance loss compared to the proposed scheme combined with the ZF digital beamforming. Second, the proposed scheme and the GS+OPA scheme are monotonically decreasing as the sum-rate requirement increases. This is because when the sum-rate requirement increases, more power should be allocated to the ID receiver for satisfying the sum-rate requirement, hence leaving less power for the EH receivers. One interesting observation is that the gap between the proposed scheme and the GS+OPA scheme becomes larger with the growing sum-rate requirement. This is because for the proposed scheme, the power allocated to different ID receivers follows the “water-filling” structure, while the greedy scheduling scheme allocates wireless power to one ID receiver only, thus resulting in a lower EH efficiency. Moreover, we plot the power allocation for all EH and ID receivers versus the sum-rate requirement in Fig. 3(c). It is observed that some power is allocated to the ID receivers to satisfy the sum-rate requirement, while a large portion of power is allocated to one EH receiver to maximize the harvested sum-power. This is in sharp contrast to the conventional far-field SWIPT case, for which all powers should be allocated to ID receivers [9].

B. Effect of Number of ID Receivers

Next, we show the effect of the number of ID receivers on the harvested sum-powers by different schemes in Fig. 3(d). Apart from the original two ID receivers, the newly added ID receivers are uniformly distributed in an area with a radius range $[1.05Z, 1.3Z]$ and a spatial angle range $[-\frac{\pi}{3}, \frac{\pi}{3}]$. First, it is observed that the proposed scheme monotonically increases with M . This is intuitively expected since when M increases, the newly added ID receivers can charge the selected EH receiver. Besides, the harvested sum-powers by both OS+EPA and AS+EPA schemes appear to decrease with M . This is because less power is allocated to the scheduled EH receiver with a larger M , thus reducing the total harvested sum-power.

VI. CONCLUSIONS

In this paper, we considered a new mixed-field SWIPT system consisting of both near-field EH receivers and far-field ID receivers. Specifically, we first formulated an optimization

problem to maximize the weighted sum-power harvested at all EH receivers by jointly optimizing the BS beam scheduling and power allocation, subject to the sum-rate and transmit power constraints. We then proposed an efficient algorithm that leverages the binary variable elimination and SCA methods to obtain a suboptimal solution. Last, numerical results are presented to validate the effectiveness of the proposed scheme against various benchmark schemes.

REFERENCES

- [1] W. Saad, M. Bennis, and M. Chen, “A vision of 6G wireless systems: Applications, trends, technologies, and open research problems,” *IEEE Network*, vol. 34, no. 3, pp. 134–142, May 2020.
- [2] Y. Liu, J. Xu, Z. Wang, X. Mu, and L. Hanzo, “Near-field communications: What will be different?” *arXiv preprint arXiv:2303.04003*, 2023.
- [3] M. Cui, Z. Wu, Y. Lu, X. Wei, and L. Dai, “Near-field MIMO communications for 6G: Fundamentals, challenges, potentials, and future directions,” *IEEE Commun. Mag.*, vol. 61, no. 1, pp. 40–46, Jan. 2023.
- [4] Y. Zhang, C. You, L. Chen, and B. Zheng, “Mixed near-and far-field communications for extremely large-scale array: An interference perspective,” *arXiv preprint arXiv:2301.07277*, 2023.
- [5] H. Zhang, N. Shlezinger, F. Guidi, D. Dardari, M. F. Imani, and Y. C. Eldar, “Beam focusing for near-field multiuser MIMO communications,” *IEEE Trans. Wireless Commun.*, vol. 21, no. 9, pp. 7476–7490, Sep. 2022.
- [6] M. Cui, L. Dai, Z. Wang, S. Zhou, and N. Ge, “Near-field rainbow: Wideband beam training for XL-MIMO,” *IEEE Trans. Wireless Commun.*, early access, 2022.
- [7] W. Liu, C. Pan, H. Ren, F. Shu, S. Jin, and J. Wang, “Low-overhead beam training scheme for extremely large-scale RIS in near-field,” *arXiv preprint arXiv:2211.15910*, 2022.
- [8] E. Björnson, Ö. T. Demir, and L. Sanguinetti, “A primer on near-field beamforming for arrays and reconfigurable intelligent surfaces,” in *2021 55th Asilomar Conference on Signals, Systems, and Computers*, 2021, pp. 105–112.
- [9] J. Xu, L. Liu, and R. Zhang, “Multiuser MISO beamforming for simultaneous wireless information and power transfer,” *IEEE Trans. Signal Process*, vol. 62, no. 18, pp. 4798–4810, Sep. 2014.
- [10] C. Pan, H. Ren, K. Wang, M. Elkashlan, A. Nallanathan, J. Wang, and L. Hanzo, “Intelligent reflecting surface aided MIMO broadcasting for simultaneous wireless information and power transfer,” *IEEE J. Sel. Areas Commun.*, vol. 38, no. 8, pp. 1719–1734, Aug. 2020.
- [11] Y. Han, S. Jin, C.-K. Wen, and X. Ma, “Channel estimation for extremely large-scale massive MIMO systems,” *IEEE Wireless Commun. Lett.*, vol. 9, no. 5, pp. 633–637, May 2020.
- [12] C. You, B. Zheng, and R. Zhang, “Fast beam training for IRS-assisted multiuser communications,” *IEEE Wireless Commun. Lett.*, vol. 9, no. 11, pp. 1845–1849, Nov. 2020.
- [13] Y. Zhang, X. Wu, and C. You, “Fast near-field beam training for extremely large-scale array,” *IEEE Wireless Commun. Lett.*, vol. 11, no. 12, pp. 2625–2629, Dec. 2022.
- [14] J. Chen, F. Gao, M. Jian, and W. Yuan, “Hierarchical codebook design for near-field mmwave MIMO communications systems,” *arXiv preprint arXiv:2212.07847*, 2022.
- [15] X. Mu, Y. Liu, L. Guo, J. Lin, and N. Al-Dhahir, “Exploiting intelligent reflecting surfaces in NOMA networks: Joint beamforming optimization,” *IEEE Trans. Wireless Commun.*, vol. 19, no. 10, pp. 6884–6898, Oct. 2020.